

CORROSION PROPERTIES OF DIFFERENT FORMS OF CARBON STEEL IN SIMULATED CONCRETE PORE WATER

KOROZIJSKE LASTNOSTI RAZLIČNIH OBLIK JEKEL V SIMULIRANI PORNJI VODI BETONA

Aleš Česen¹, Tadeja Kosec¹, Andraž Legat¹, Violeta Bokan-Bosiljkov²

¹Slovenian National Building and Civil Engineering Institute, Dimičeva 12, 1000 Ljubljana, Slovenia
²Faculty of Civil and Geodetic Engineering, University of Ljubljana, Jamova cesta 2, 1000 Ljubljana, Slovenia
ales.cesen@zag.si

Prejem rokopisa – received: 2013-03-13; sprejem za objavo – accepted for publication: 2013-04-23

Carbon steel, such as concrete-reinforcing steel, tends to undergo corrosion processes when exposed to certain environmental actions. These are the carbonation of concrete and the ingress of chlorides into the concrete from the environment. Many times, the carbonation and chloride contamination are simultaneous processes leading to a harsh corrosion environment and subsequent corrosion problems. Monitoring the state of corrosion is thereby a very useful and powerful tool for following and evaluating the lifetime of reinforced concrete structures. Electrochemical measurements were performed to investigate different forms of carbon steel in simulated concrete pore water at different pH values with and without the presence of chlorides. Morphological characteristics of three different types of carbon steel were studied and SEM/EDX and Raman analyses of the corrosion products were performed. It was found that steel in the form of a sheet has a higher corrosion resistivity than a steel wire and a steel rod, and that the steel rod has a higher corrosion resistivity than the steel wire. The corrosion layer on carbon steel is very diverse; several morphologies were found and analyzed.

Keywords: carbon steel, metallography, corrosion, concrete pore water

Maloogljčno jeklo, kot je jeklena betonska armatura, je izpostavljeno korozivnim procesom zaradi vplivov okolja. To sta karbonatizacija betona ter vdor kloridnih ionov iz okolja. Mnogokrat se karbonatizacija in vdor kloridov zgodi istočasno, kar privede do hitrega korozivnega propadanja. Spremljanje korozije na objektih je zato zelo dobro orodje za napoved in oceno preostanka trajnostne dobe nekega objekta. Elektrokemijske preiskave smo izvedli v simulirani raztopini porne vode v betonu pri različnih pH vrednostih ter brez in v prisotnosti kloridnih ionov. Določili smo mikrostrukturne značilnosti posameznih vrst ogljičnih jekel ter morfologijo korozivnih produktov z EDX/SEM-analizo ter Ramansko spektroskopijo. Ugotovili smo, da je najbolj korozivno odporno ogljično jeklo v obliki folije, sledi palica, najslabše korozivne lastnosti pa ima žica iz ogljičnega jekla. Korozivni produkti na jeklu so različnih morfoloških oblik in sestav.

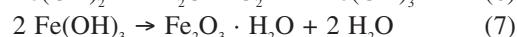
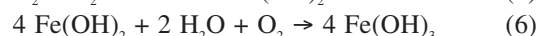
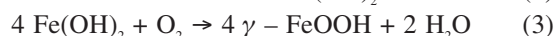
Ključne besede: ogljično jeklo, metalografija, korozija, porna voda betona

1 INTRODUCTION

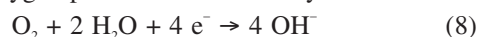
The service life of a reinforced concrete structure depends on the corrosion state of the reinforcing steel that is embedded in the concrete.¹ There are numerous ways to prolong the service life of a structure, among them also the measures related to the properties of structural materials such as using high-performance concretes with improved properties²⁻⁴ or using a more durable reinforcement material like the corrosion-resistant steel.⁵⁻¹⁰ However, the use of the common carbon steel as a concrete reinforcement is still the most frequent and economical. Thus, reliable corrosion monitoring is essential to assess the remaining life-time of a structure, to help select an optimum rehabilitation process and evaluate its efficiency.¹⁰⁻¹² With a corrosion monitoring system we aim to detect the changes in the reinforcement condition, evaluate the corrosion rates and determine the types and causes of corrosion.¹³⁻¹⁵

It is of great importance to know the corrosion stages and mechanisms in order to evaluate the intensity of corrosion. Thereby, two extreme conditions were chosen

to be studied in the present research. These are the ingress of chloride ions and the carbonation of the cement matrix. At a high alkalinity and high pH, the passive film on the carbon steel protects the metal from corrosion.¹³ The oxide layer consists of firm and adherent Fe₂O₃.¹³ When the same steel is subjected to a low pH, or a pore solution containing chlorides, the passivity is lost. Anodic reactions of carbon steel are dissolving iron through many possible reactions:



The cathodic reaction in such cases can be a reduction of the oxygen present in the electrolyte:



On the other hand, carbon dioxide can reduce the protective role of concrete due to a reaction with the

hydrated cement paste, leading to a pH decrease and a subsequent loss of passivity and to a corrosion initiation.^{13,16} The corrosion reaction in such an environment is accelerated.

The aim of the present study is to compare the corrosion properties of different forms of carbon steel, differing by their microstructural properties. Their corrosion properties in a simulated concrete-pore-water solution are also evaluated with the presence of chloride ions. Different spectroscopic techniques are used to study morphological and mineralogical characteristics of the corrosion products on steel.

2 EXPERIMENTAL WORK

2.1 Materials and surface preparation

Three types of samples were chosen for the study, namely:

- 1) Carbon-steel sheets 240 μm thick with the sections of different dimensions. The wire for the electrical contact on the carbon-steel-sheet specimen was attached at the side of the sheet plates beforehand. It was protected by epoxy paint.
- 2) Carbon-steel rods with a diameter of 5.0 mm. The wire for the electrical contact was attached at the top of the rod prior to the measurements.
- 3) Carbon-steel wires with a diameter of 0.8 mm. The cross-section of the wire was exposed to the electrolyte.

Before each measurement, the wires and steel rods were abraded with the 1200-grit emery paper, degreased with acetone and then well dried.

2.2 Electrochemical measurements

The electrochemical measurements were performed in different types of the solution:

- 1) the 0.01 M calcium hydroxide solution, simulating the concrete pore water at pH 12.8
- 2) the 0.01 M sodium tetraborate solution, simulating the pore water of the carbonated concrete and a presence of chloride ions (pH 9.2, containing 0.58 % of NaCl)

A laboratory-made three-electrode corrosion cell was used with an approximate volume of 300 cm^3 . The specimen was prepared in such a way that the exposed surface presented the working electrode. For the electrochemical tests a potentiostat/galvanostat PGSTAT100, the floating version, Metrohm, Netherlands, 2010, expanded with the NOVA module was used.

After the initial stabilization 2 h at the open-circuit potential (OCP), 3 subsequent linear polarization measurements at ± 20 mV vs. OCP with a scan rate of 0.1 mV/s were performed. Finally, the potentiodynamic curve was measured in the range of -250 mV vs. OCP to 0.6 V at a scan rate of 1 mV/s.

2.3 SEM/EDX analysis

For the SEM/EDX analysis, a sample of the carbon-steel sheet was embedded into the cement mortar. The carbon-steel sheet was exposed to wetting and drying cycles during a 12-week exposure. During the first 6 weeks, the cycle period consisted of 2 days of wetting with distilled water and 5 days of drying the mortar specimen. During the second 6-week period, the cycles consisted of wetting the specimen with a 3.5 % NaCl solution. After the exposure, the mortar was detached from the steel-sheet sensor and the corrosion products were investigated using SEM and EDS. At the end of the exposure, the carbon-steel sheet was detached from the mortar cover, rinsed with distilled water and dried. The surface morphology was inspected and analyzed with a low-vacuum scanning electron microscope (SEM, JSM 5500 LV, JOEL, Japan) at the acceleration voltage of 20 kV. The microscope was equipped with energy dispersive spectroscopy (Inca, Oxford Instruments Analytical, UK). The EDS analysis was performed at the acceleration voltage of 20 kV.

2.4 Raman analysis

The Raman spectra were obtained with a Horiba Jobin Yvon LabRAM HR800 Raman spectrometer coupled with an Olympus BXFM optical microscope. The measurements were performed using a laser excitation line 633 nm, a 100-times objective lens and a 600-grooves per millimetre grating, which gave a spectral resolution of 2 cm^{-1} per pixel. The power of the laser was set at 0.14 mW. A multi-channel air-cooled CCD detector was used, with the integration times of between 20 s and 30 s. The spectra presented are without any baseline correction.

2.5 Metallographic examination

The samples were first grinded up to grades 2000, then they were polished up to 4000 and finally a paste 0.5 μm was used. The etching for uncovering the microstructure was performed in a 3 % mixture of HNO_3 in ethanol for 20 s. The samples were then immediately rinsed with ethanol and dried with air. A CARL ZEISS AXIO Imager M2m optical metallographic microscope was used to study the microstructure of the steel specimens. Metallographic specimens were prepared and investigated in the longitudinal and transverse directions of the castings. The results of the directions representing the exposed surfaces in the electrochemical study were obtained.

3 RESULTS AND DISCUSSION

In order to evaluate the corrosion properties of the three different types of carbon steel, electrochemical

experiments were conducted in a simulated concrete-pore-water solution with pH 12.8.

The comparison of the electrochemical properties at pH 12.8 and the ones in the simulated carbonated environment at pH 9.2 and with the presence of 0.58 % of chlorides is presented as well. For a further evaluation of the corrosion behavior, the samples were characterized after a 12-week exposure to the cycling conditions. After that, the surface of the exposed sensor from the carbon-steel sheet was examined with EDX/SEM and the Raman technique.

3.1 Metallographic examination

Metallographic images of the three shapes of the steel specimens are presented in **Figure 1**, namely, a longitudinal view of the steel sheet (a), the rod (b) and a cross-section of the wire (c).

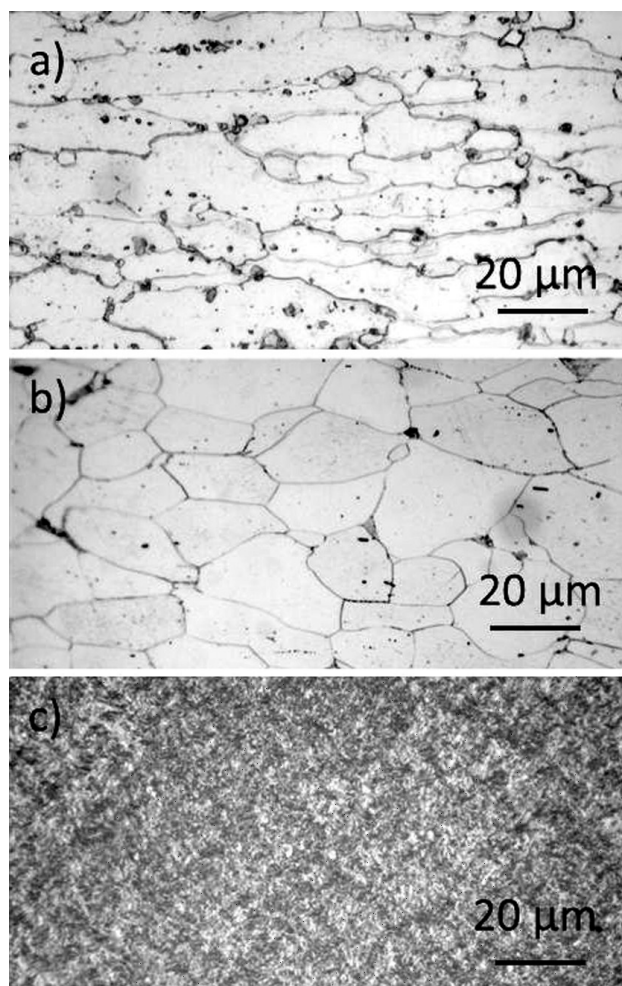


Figure 1: Metallographic images of the three forms of carbon steel: a) steel sheet – a longitudinal view, b) steel rod – a longitudinal view, c) steel wire – a cross-section

Slika 1: Metallografski posnetki treh različnih oblik ogljičnega jekla: a) vzdolžni prežek jeklene plošče, b) vzdolžni prežek jeklene palice in c) prežek žice

The steel sheet has a well-defined microstructure. It consists of ferrite crystal grains that vary in size from 20 μm to 40 μm (**Figure 1a**). Small spheroid-shaped carbides are distributed at the edges and in the crystal grains. It is assumed that the carbides might affect the corrosion properties of the steel sheet.

The microstructure of the rod in the longitudinal direction is mostly ferritic (**Figure 1b**). The amount of perlite is very small due to a low carbon content. Crystal grains are of the size of between 20 μm and 45 μm and are extremely pure towards the surface of the normalized steel rod. The content of the sulfide inclusions increases towards the core of the rod.

The cross-section of the wire has a lamellar microstructure due to the cold-worked procedure (**Figure 1c**). The microstructure consists of cementite and ferrite that were induced out of the perlite microstructure. The size of the cementite lamellas is estimated to be several nanometres.¹⁷ The corrosion performance of the wire is expected to be more susceptible to corrosion in the cross-section than in the longitudinal direction.

3.2 Electrochemical measurements

During the stabilization process, the open-circuit potential was measured as a function of time. **Figure 2** represents the open-circuit potential curves of the three different types of the steel specimens, namely, the carbon sheet, the carbon-steel rod and the carbon-steel wire, immersed in a simulated concrete-pore-water solution with pH 12.8. All the measured curves showed a similar electrochemical behavior.

The corrosion potential, E_{corr} , in all the cases moved to more negative values. After two hours of the immersion it stabilized at -0.280 V for the carbon-steel sheet and at -0.279 V for the carbon-steel wire. The corrosion potential of the carbon-steel rod was the lowest and

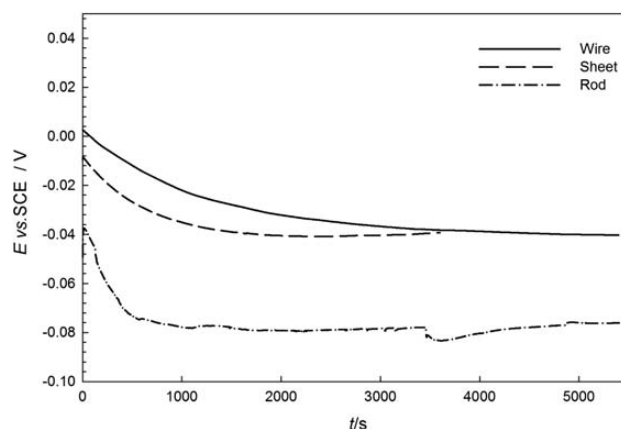


Figure 2: Open-circuit potential measurements for the three forms of carbon steel: steel sheet, steel rod and steel wire, immersed in simulated pore water, pH 12.5

Slika 2: Meritve pri potencialu odprtega kroga za jekleno ploščo, jekleno palico in prežek žice, potopljene v simulirano raztopino betona, pH 12,5

stabilized at -0.315 V after two hours of the immersion. The observed decrease in the value of E_{corr} in time might be a result of the formation of an adsorbed layer at the interface of the carbon steel/electrolyte in the simulated concrete-pore-water solution. However, the E_{corr} evolution is quite regular, indicating that a stable layer was formed on the investigated steel surfaces. The corrosion potentials, E_{corr} , are relatively high, since the corrosion potentials of corroding steels are reported to be as low as -0.7 V.¹⁶

At a low pH and in a chloride-contaminated environment, the corrosion potentials moved to a more negative direction (Figure 3). After a exposure 1 h, it was -0.5605 V for the steel sheet, -0.620 V for the wire and -0.624 V for the rod. The lower values for all the investigated samples, compared to the values at pH 12.8, point at a loss of passivity.

The exposed surfaces, as in the exposure of different types of specimens to the concrete environment, were tested in the course of the electrochemical testing. Namely, the cross-section of the wire, the outer surface of the rod and the sheet were exposed to the simulated pore water with a high alkalinity and to the pore water with pH 9.2, containing 0.58 % of NaCl in order to simu-

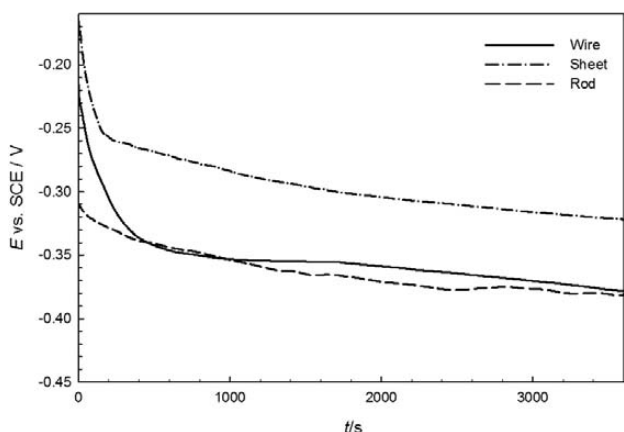


Figure 3: Open-circuit potential measurements for the three forms of carbon steel: steel sheet, steel rod and steel wire, immersed in simulated pore water with pH 9.2, containing 0.58 % of chlorides

Slika 3: Meritve pri potencialu odprtega kroga za jekleno ploščo, jekleno palico in prevez žice, potopljene v simulirano raztopino betona, pH 9.2 z 0.58 % kloridov

Table 1: Corrosion potential, polarization resistance and corrosion rates for the carbon-steel sheet, carbon-steel wire and rod. E_{corr} and E_b are the values deduced from the potentiodynamic measurements.

Tabela 1: Korozijski potencial, polarizacijska upornost in korozijska hitrost za jekleno ploščo, žico in palico. Vrednosti E_{corr} in E_b so odčitane iz potenciodinamskih meritvev.

	pH = 12.8			pH = 9.2 + 0.58 % NaCl		
	wire	sheet	rod	wire	sheet	rod
$E_{\text{corr}} / \text{V}$	-0.279	-0.280	-0.312	-0.62	-0.56	-0.62
$R_p / (\text{k}\Omega \text{ cm}^2)$	246	2014	1260	0.39	2.10	1.33
E_b / V	0.653	0.683	0.648	-0.422	-0.027	-0.099
$v_{\text{corr}} / (\mu\text{m}/\text{year})$	1.3	0.16	0.24	773	143	227

late a carbonated and chloride-contaminated environment.

The corrosion potential was measured until it reached a steady state, followed by a potentiodynamic linear polarization and a wide potential scan at a higher scan rate.

The corrosion potential after a exposure 2 h to the pore water with a high pH shows minimum differences among different samples. The results are presented in Table 1. However, when exposed to the pore water with pH 9.2, containing chlorides, the corrosion potential changes and moves towards more negative values by approximately 300 mV.

The linear-polarization technique showed that in the simulated pore water, the surface of the steel sheet shows the highest polarization resistance of $2014 \text{ k}\Omega \text{ cm}^2$ (Table 1), followed by the carbon-steel rod ($1260 \text{ k}\Omega \text{ cm}^2$) and the cross-section of the wire ($246 \text{ k}\Omega \text{ cm}^2$). With pH 9.2, the polarization resistance, R_p , for all the inve-

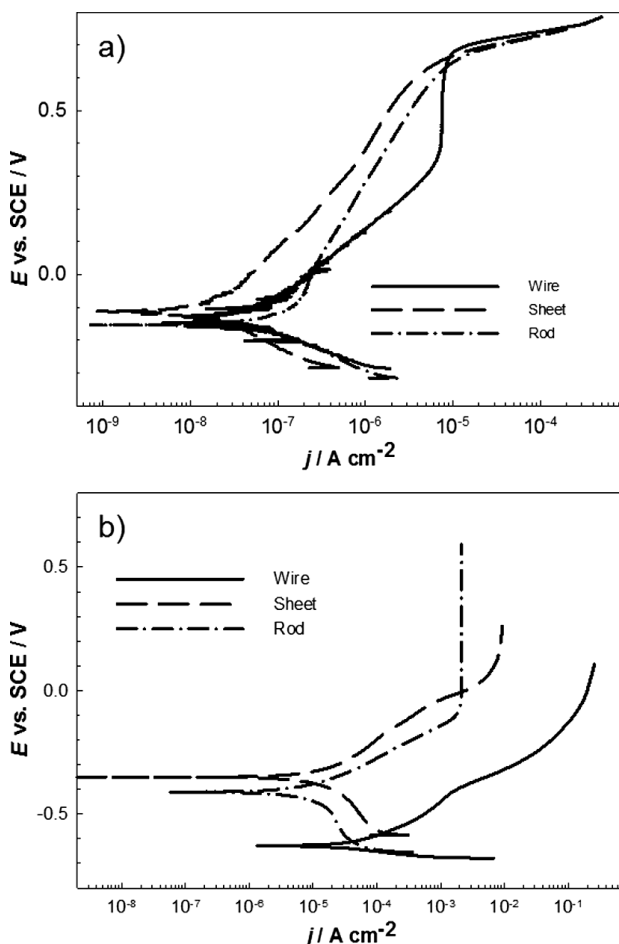


Figure 4: Potentiodynamic measurements for the three forms of carbon steel: steel sheet, steel rod and steel wire, immersed in simulated pore water, pH 12.5, and simulated pore water with pH 9.2, containing 0.58 % of chlorides at a scan rate of 0.1 mV/s

Slika 4: Meritve linearne upornosti za jekleno ploščo, jekleno palico in prevez žice, potopljene v simulirano raztopino betona, pH 12.5 in simulirano raztopino betona, pH 9.2 z 0.58 % kloridov pri hitrosti preleta 0,1 mV/s

stigated samples became smaller, since they underwent corrosion processes. It is 595 times lower than at a high alkalinity for the steel wire, 893 times lower for the steel sheet and 840 times lower for the rod. Thereby, a lower pH and a presence of chlorides greatly affect the corrosion resistance of the exposed steel surfaces. In an aggressive environment, the aggressive species have no preferential effect on the corrosion properties of different investigated microstructures since the change in the corrosion rate is very similar for all the samples.

In **Figure 4**, the potentiodynamic curves of the three surfaces and three different microstructures (**Figure 1**) are presented. There are small, but not negligible differences in the electrochemical properties in the simulated pore water at pH 12.8 (**Figure 4a**).

The corrosion-current density is as high as $j_{\text{corr}} = 0.123 \mu\text{A}/\text{cm}^2$ for the rod and $j_{\text{corr}} = 0.053 \mu\text{A}/\text{cm}^2$ for the cross-section of the wire. The carbon-sheet sample exhibits the lowest corrosion-current density ($j_{\text{corr}} = 0.017 \mu\text{A}/\text{cm}^2$). The current densities in the pseudo passive region in the anodic scans are the lowest for the steel sheet, followed by the rod, and the highest currents are found for the wire. The breakdown potentials are similar at 0.65 mV vs. SCE (the results are presented in **Table 1**).

At a lower pH, the potentiodynamic curves are different for different samples. The corrosion potentials move towards negative values, the corrosion-current densities decrease and the breakdown potentials change. The corrosion-current density is the highest for the carbon wire ($j_{\text{corr}} = 19.1 \mu\text{A}/\text{cm}^2$), smaller for the rod ($j_{\text{corr}} = 7.72 \mu\text{A}/\text{cm}^2$) and the smallest for the carbon sheet ($j_{\text{corr}} = 3.78 \mu\text{A}/\text{cm}^2$). Also, the breakdown potentials become smaller as observed from the potentiodynamic curves and the values given in **Table 1**.

Following that, the corrosion rates were estimated. Any possible instances of crevice corrosion were elimi-

nated, so the corrosion rates were deduced from the linear polarization using an equation, where the corrosion rate, v_{corr} , in $\mu\text{m}/\text{year}$ is calculated following the Faraday law¹⁸:

$$v_{\text{corr}} = 3.27 \cdot (j_{\text{corr}} \cdot w/M) / (d \cdot n)^{-1} \quad (9)$$

where j_{corr} stands for the corrosion-current density in $\mu\text{A cm}^{-2}$, d is the density of the metal in g cm^{-3} , w is the atomic mass (without units) and n is the number of exchanged electrons. The steel density is $d = 7.8 \text{ g cm}^{-3}$ and the equivalent mass is $w/M = 58$.

j_{corr} was calculated from the equation, using the Stern-Geary approximation of the Tafel coefficients:

$$j_{\text{corr}} = 1/2.303 \cdot R_p (\beta_A \cdot \beta_C / (\beta_A + \beta_C)) \quad (10)$$

with β_A and β_C being 120 mV per decade.

As observed from these measurements, the corrosion rate is low at a high alkalinity and it increases immensely at a lower pH, especially when chlorides are introduced. The effect of the microstructure is reflected in the corrosion performance. The carbon-steel sheet sample has better corrosion properties than the carbon-steel rod, whereas the carbon-steel wire is the most sensitive to corrosion processes.

3.3 Surface characterization using SEM/EDX and the Raman analysis

Different morphologies of corrosion products were found on the steel surface: compact doughnut-type corrosion products (**Figure 5a**), fine rounded particles as presented in **Figure 5b**, a compact structure with visible cracks in the surface (**Figure 5c**) and rounded particles with a greater diameter (**Figure 5d**).

All the identified corrosion products are iron-based oxides or oxyhydroxides, some of them containing traces of chlorine (**Table 2**).

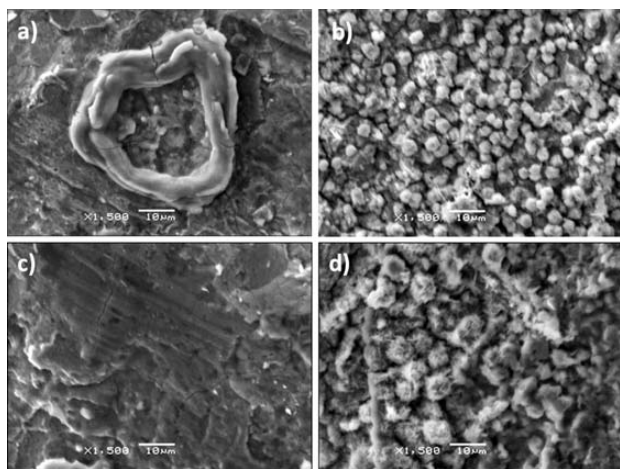


Figure 5: SEM images of the corrosion products on the carbon-steel sheet after a 12-week exposure to wet and dry cycles in the mortar
Slika 5: SEM-prikaz korozivskih produktov po 12-tedenski izpostavitvi cikliranem močenju in sušenju v karbonatizirani malti

Table 2: Mass fractions (w/%) of different elements in the corrosion products on the steel sheet

Tabela 2: Masni delež (w/%) različnih elementov v korozivskih produktih, najdenih na jekleni plošči

product	Fe	O	Na	Cl	Al	Si
a	25.15	72.13		2.29	0.43	
b	21.42	71.78	6.58	0.22		
c	31.03	61.56		0.44	0.76	0.89
d	33.17	58.89	4.25	2.59	0.79	0.30

The Raman analysis was also conducted on the steel corrosion products. Since it is very difficult to link the morphologies, found on SEM, with the optical magnifications, it was not possible to unambiguously recognize each shape. The Raman spectra are presented in **Figure 6**.

Different types of iron oxides were identified. These are hematite, lepidocrocite, gheothite, maghemite and akaganeite. Different Raman spectra of the corrosion

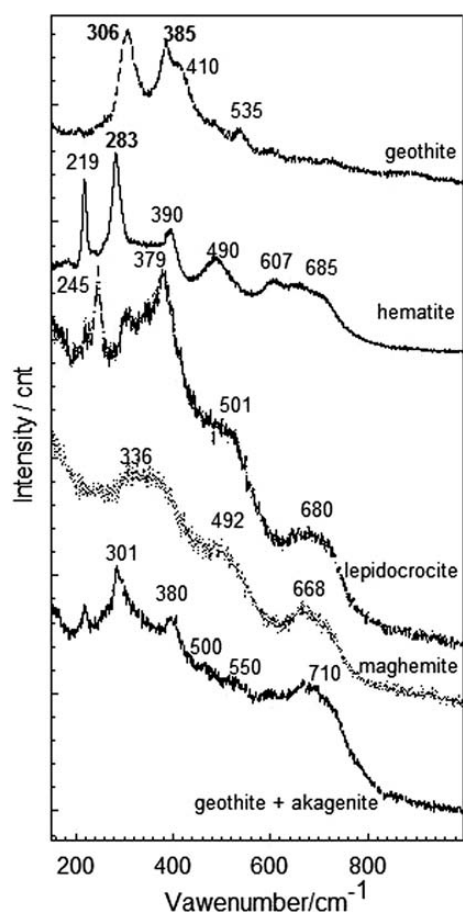


Figure 6: Raman spectra of different corrosion products on the steel-sheet surface

Slika 6: Ramanski spekter različnih korozijskih produktov na jekleni pločevini

products found on the steel-sheet surface are presented in **Figure 6**.

Geothite is characterized by two strong bands at 306 cm^{-1} and 385 cm^{-1} . The latter is broadened as a shoulder of the peak at 410 cm^{-1} . There is a weak band at 535 cm^{-1} . Geothite is an α - FeOOH , iron oxyhydroxide, transparent and with an orthorhombic structure. The spectra were found in the literature.¹⁹ Hematite is defined by two strong bands at 219 cm^{-1} and 283 cm^{-1} and three weak and broad bands at (390, 490, 607 and 685) cm^{-1} . The results are similar to those reported in^{19,20}.

Lepidocrocite, a γ - FeOOH polymorph of iron oxyhydroxide, usually detected as a ruby-red corrosion product, was detected at several points with the characteristic bands at 245 cm^{-1} , 303 cm^{-1} , 379 cm^{-1} , 501 cm^{-1} and 680 cm^{-1} . Similar spectra were already reported.¹⁹

Maghemite, γ - Fe_2O_3 , can be identified by broad and non-intensive bands at 336 cm^{-1} , 492 cm^{-1} and 668 cm^{-1} . This corrosion product is the most prevalent on the examined surface.

At several spots, mixtures of different corrosion products were found, for example, a mixture of geothite and akagenite. In the Raman spectra in **Figure 6**, only the

bands characteristic for akagenite are denoted. These are (301, 380, 500, 550 and 710) cm^{-1} , whereas the most pronounced geothite bands appear at (285, 399 and 534) cm^{-1} .

The corrosion products on the steel-carbon sheet embedded in the mortar are very versatile. They were investigated with SEM and their mineralogical nature was identified with the Raman analysis. They consist of different iron oxides and oxyhydroxides.

4 CONCLUSIONS

Corrosion properties of three different forms of carbon steel were investigated using metallography, electrochemical and surface-spectroscopic techniques.

It was found that the microstructures of the three investigated samples are different. This has an important effect on the electrochemical properties of different samples of carbon steel.

At a high alkalinity of the simulated concrete-pore-water solution with pH 12.8, the corrosion rates are low and similar, while the effect of the microstructure is still observed. The lowest corrosion rate was found for the carbon-steel sheet, followed by the carbon-steel rod and the wire, respectively. The microstructure of the wire is the most sensitive one.

In the carbonated environment, in the concrete pore water with pH 9.2, containing chlorides, the electrochemical properties of the investigated samples change immensely. The corrosion proceeds and the corrosion rate increases, causing a more expressed sensitivity of the microstructure. The highest corrosion rate was found for the wire that has the most sensitive microstructure, followed by the carbon-steel rod and the sheet, respectively.

Different and versatile corrosion products were found on the steel-carbon sheet embedded in the cement mortar after an exposure to wet and dry cycles. They were investigated with SEM and their mineralogical nature was identified with the Raman analysis. Different iron oxides and oxyhydroxides were identified, such as geothite, lepidocrocite, hematite, maghemite and akagenite.

Acknowledgment

The help of Petra Močnik with laboratory experiments is greatly acknowledged as well as the help of Viljem Kuhar with the metallographic analysis and helpful discussions.

5 REFERENCES

- ¹ P. K. Mehta, P. J. M. Monteiro, Concrete: microstructure properties and materials, McGraw-Hill, New York 2006
- ² P. Dinakar, K. G. Babu, M. Santhanam, Corrosion behaviour of blended cements in low and medium strength concretes, Cement and Concrete Composites, 29 (2007), 136–145

- ³ J. Tritthart, Transport of a surface-applied corrosion inhibitor in cement paste and concrete, *Cement and Concrete Research*, 33 (2003), 829–834
- ⁴ L. G. Andión, P. Garcés, F. Cases, C. G. Andreu, J. L. Vazquez, Metallic corrosion of steels embedded in calcium aluminate cement mortars, *Cement and Concrete Research*, 31 (2001), 1263–1269
- ⁵ A. Šajna, A. Legat, D. Bjegović, T. Kosec, I. Stipanović, M. Serdar, V. Kuhar, N. Gartner, L. Pardi, L. Augustynski, Recommendations for the use of corrosion resistant reinforcement, FEHRL 79, Brussels, 2009
- ⁶ D. Addari, B. Elsener, A. Rossi, Electrochemistry and surface chemistry of stainless steels in alkaline media simulating concrete pore solutions, *Electrochim. Acta*, 53 (2008), 8078–8086
- ⁷ C. M. Abreu, M. J. Cristobal, R. Losada, X. R. Novoa, G. Pena, M. C. Perez, High frequency impedance study of passive films formed on 316 stainless steel in alkaline medium, *J. Electroanal. Chem.*, 572 (2004), 335–345
- ⁸ A. Bautista, G. Blanco, F. Velasco, A. Gutierrez, L. Soriano, E. J. Palomares, H. Takenouti, Changes in the passive layer of corrugated austenitic stainless steel of low nickel content due to exposure to simulated pore solutions, *Corros. Sci.*, 51 (2009), 785–792
- ⁹ M. C. Garcia-Alonso, M. L. Escudero, J. M. Miranda, M. I. Vega, F. Capilla, M. J. Correia, M. Salta, A. Bennani, J. A. Gonzales, Corrosion behaviour of new stainless steel reinforcing bar embedded in concrete, *Cement Concrete Res.*, 37 (2007), 1463–1471
- ¹⁰ I. Martínez, C. Andrade, Examples of reinforcement corrosion monitoring by embedded sensor in concrete structure, *Cement Concrete Comp.*, 31 (2009), 545–554
- ¹¹ G. S. Duffo, S. B. Farina, Development of an embeddable sensor to monitor the corrosion process of new and existing reinforced concrete structures, *Constr. Building Mat.*, 23 (2009), 2746–2751
- ¹² A. Legat, Monitoring of steel corrosion in concrete by electrode arrays and electrical resistance probes, *Electrochim. Acta*, 52 (2007), 7590–7598
- ¹³ L. Bertolini, B. Elsener, P. Pedferri, R. B. Polder, *Corrosion of Steel in Concrete: Prevention, Diagnosis, Repair*, Wiley-VCH Verlag GmbH & Co, Weinheim 2004
- ¹⁴ A. Bentour, S. Diamond, N. S. Berke, *Steel Corrosion in Concrete*, E & FN Spon, an imprint of Chapman & Hall, 2-6 Boundary Row, London 1997
- ¹⁵ P. Pedferri, L. Bertolini, M. Gastaldi, T. Pastore, M. P. Pedferri, *Stainless Steel in Concrete*, European Community, COST 521 Workshop, Utrecht, 1998
- ¹⁶ J. P. Broomfield, *Corrosion of steel in concrete: understanding, investigation and repair*, Taylor & Francis, Florence 2007
- ¹⁷ A. Milenin, Z. Muskalski, The FEM simulation of cementite lamellas deformation in pearlitic colony during Drawing of High Carbon Steel, 1375–1380, In: J. M. A. Cesar de Sa, A. D. Santos (eds.), *Materials Processing and Design: Modeling, Simulation and Applications*, Numiform 2007: Proceedings of the 9th International Conference on Numerical Methods in Industrial Forming Processes, American Institute of Physics, 2007
- ¹⁸ B. Elsener, Corrosion rate of steel in concrete – Measurements beyond the Tafel law, *Corros. Sci.*, 47 (2005), 3019–3033
- ¹⁹ F. Dubois, C. Mendibide, T. Pagnier, F. Perrard, C. Durret, Raman mapping of corrosion products formed onto spring steels during salt pray experiment, a correlation between the scale composition and the corrosion resistance, *Corros. Sci.*, 50 (2008), 3401–3409
- ²⁰ W. Chen, R. G. Du, C. Q. Ye, Y. F. Zhu, C. J. Lin, Study on the corrosion behaviour of reinforcing steel in simulated concrete pore solution using in situ Ramanspectroscopy assisted by electrochemical techniques, *Electrochim. Acta*, 55 (2010), 5677–5682